(Preprint) AAS 15-802

SEASONAL VARIATIONS OF THE JAMES WEBB SPACE TELESCOPE ORBITAL DYNAMICS

Jonathan Brown,[*] Jeremy Petersen,[†] Benjamin Villac,[‡] and Wayne Yu[§]

While spacecraft orbital variations due to the Earth's tilt and orbital eccentricity are well-known phenomena, the implications for the James Webb Space Telescope present unique features. We investigate the variability of the observatory trajectory characteristics, and present an explanation of some of these effects using invariant manifold theory and local approximation of the dynamics in terms of the restricted three-body problem.

INTRODUCTION

The James Webb Space Telescope (JWST) is a flagship mission scheduled for launch in 2018, and it will be the scientific successor to the Hubble Space Telescope and the Spitzer Space Telescope. The project is an international collaboration between National Aeronautics and Space Administration (NASA), the European Space Agency (ESA), and the Canadian Space Agency, and NASA Goddard Space Flight Center is managing the development. The JWST mission will focus on the infrared spectrum in order to detect the redshifted light from very early in the universe, which will fill a gap in the current range of astrophysical observations and allow the exploration of a whole new set of fundamental scientific questions ranging from the formation of the universe to the origin of planetary systems.

Given the sensitivity of the instruments to stray light, the mission will orbit in the vicinity of the Sun-Earth/Moon L2 libration point, allowing the optical element to remain pointed away from the Sun, the Earth, and the Moon at all times. The near constant geometry of the trajectory relative to the Earth as it orbits about the Sun allows the observatory to map large swaths of the celestial sphere while providing long-duration communication links to the Earth. The orbital dynamics in the L2 region also support the spacecraft mass-budget constraints with minimal transfer and orbit maintenance costs, as well as slightly reduced irradiation from the Sun and less magnetospheric contamination as compared to a low-Earth orbit. Thermal constraints on the instruments impose the need for a 163 square-meter sunshield as shown in Figure 1, the presence of which significantly couples the orbital and attitude dynamics as the Sun's rays impinge on this surface. In addition to the need for the sunshield, thermal requirements also prevent the placement of thrusters on the instrument side of the observatory; thus no Sun-ward maneuvers are allowed, which tightly couples

[*] Sr. Systems Engineer, Mission Engineering and Technologies Division, a.i. solutions, Inc., 10001 Derekwood Ln. Ste. 215, Lanham, MD 20706.
[†] Systems Engineer, Mission Engineering and Technologies Division, a.i. solutions, Inc., 10001 Derekwood Ln. Ste. 215, Lanham, MD 20706.
[‡] Pr. Systems Engineer, Mission Engineering and Technologies Division, a.i. solutions, Inc., 10001 Derekwood Ln. Ste. 215, Lanham, MD 20706.
[§] Flight Dynamics Engineer, Navigation and Mission Design Branch, NASA Goddard Space Flight Center, 8800 Greenbelt Rd, Greenbelt, MD 20771.

the possible science orbits and their transfer trajectories to the launch date. Shadows, or eclipses of the spacecraft by either the Earth or the Moon, are not permitted at all during the mission. All of these constraints conspire to limit the maneuverability of the spacecraft and couple the orbital dynamics to the rhythms of the Earth, Moon, and Sun.

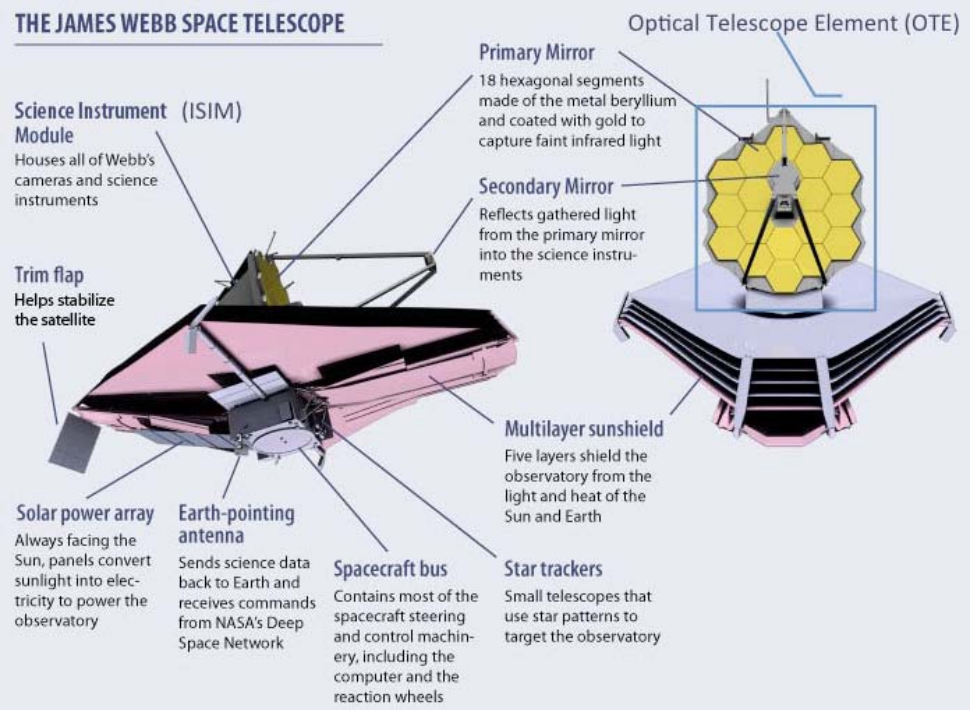

Figure 1. JWST spacecraft overview.[*]

The limitations resulting from the spacecraft design are counter-balanced by the science focus of the mission, which imposes few restrictions on the type of libration point orbit (LPO). The mission only requires the orbit to remain within a (relatively large) region in the vicinity of L2 for a 5 year operational mission (with a goal of 10 years) following the 6 month commissioning phase. While the project schedule is geared toward an October 2018 launch date, the variability in possible trajectories must be taken into account in any analysis. As such, three reference orbits, shown in Figure 2, are currently used for analysis. These trajectories are represented in the L2-centered rotating libration point (RLP) coordinate system; the X axis points from the Sun to the Earth-Moon barycenter, the Z axis points to the north ecliptic pole, and the Y axis completes the right handed system. Note in particular that the orbits resemble a northern or southern quasi-halo that shifts geometry over time. This paper aims to provide an overview of such orbital variations with launch epoch and to extract the underlying dynamical mechanisms driving such phenomena.

This paper builds on the previous detailed analysis of individual phases of the mission. Launch opportunities which satisfy all mission requirements have been computed for the 14 months following the nominal launch date of October 2018.[1] In particular, the observed effects of the various mission constraints on the launch window have been discussed and include a reduction of launch opportunities due to the Moon's influence and around the solstices. While the presence of the Moon

[*] Image credit: http://jwst.nasa.gov/observatory.html [accessed 19 May 2015]

explains some of these observations, a more detailed explanation of some of these observed variations was not addressed in that paper.

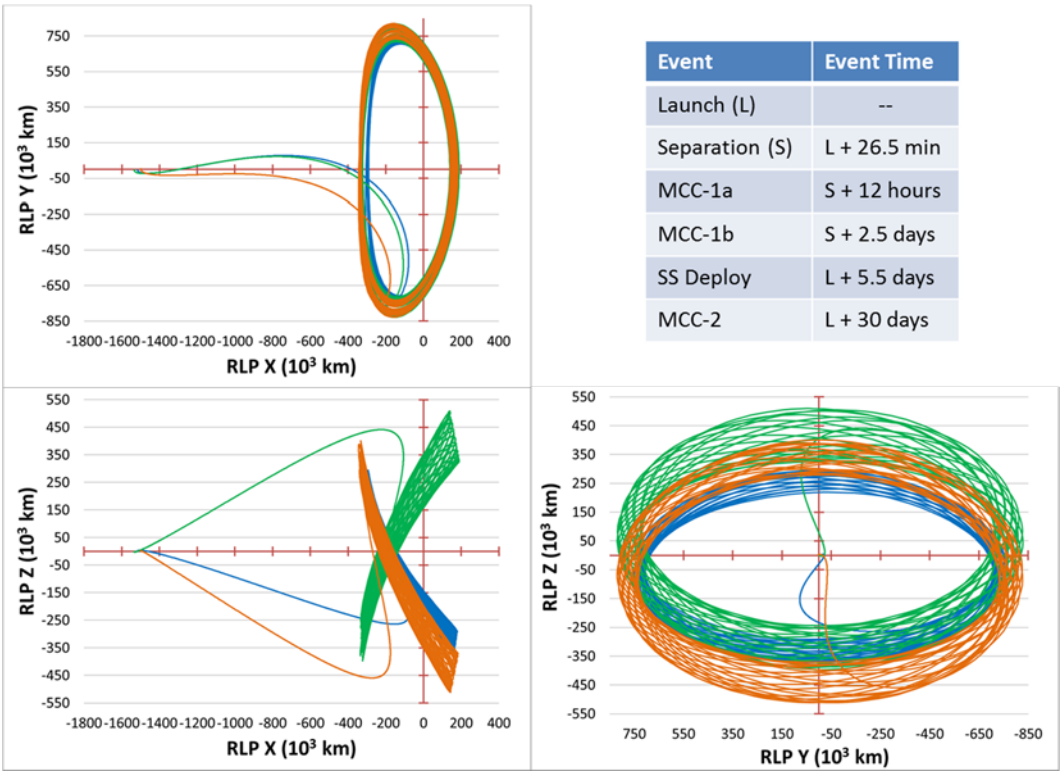

Event	Event Time
Launch (L)	--
Separation (S)	L + 26.5 min
MCC-1a	S + 12 hours
MCC-1b	S + 2.5 days
SS Deploy	L + 5.5 days
MCC-2	L + 30 days

Figure 2. JWST Design Reference Trajectories.

Complementary to this, the transfer phase has been studied, including computation and statistical analysis of the three mid-course correction (MCC) maneuvers.[2] This work described the algorithms and maneuver constraints to achieve such transfers and showed the expected dispersions of the transfer cost with respect to various model parameters. While some of these results will be reviewed here, our focus will be in explaining why such a transfer strategy leads to the observed reference trajectories that have been computed in the launch window analysis.

We show in the following that the transfers are close to ballistic, and that an underlying interpretation of the coupling of the science orbit with the launch date in terms of invariant manifolds exists. Sample science orbits can be matched with approximate orbits in the Circular Restricted Three-Body Problem (CR3BP), demonstrating the intersection of the transfer manifolds with the Earth-fixed launch insertion constraint at the epoch. As the Earth rotates on its axis, the intersection leads to daily variation in the target orbits, while the yearly eccentric motion around the Sun slowly shifts the location of these invariant manifolds relative to the insertion condition.

To proceed with this analysis, the next section reviews the main orbital constraints for the JWST mission and summarizes the observed seasonal variation phenomena during the initial mission analysis. The following section focuses on the geometry and dynamics of an approximating CR3BP model and the relation of the JWST orbit transfer with invariant manifolds of period and quasi-periodic orbits.

JWST ORBIT CONSTRAINTS AND VARIATIONS OVERVIEW

This section overviews the main constraints and observed orbital variation phenomena in analyzing the full range of launch opportunities. First the insertion condition is reviewed, followed by the transfer limitations and an overview of the launch window analysis. The observed variations are the drivers for the subsequent analysis, but the constraints also provide a first hint at their cause.

Insertion State Constraint

ESA will provide an Ariane 5 launch vehicle which, after departing Kourou, French Guiana, will inject JWST into a highly eccentric orbit.[1] There are three possible flight programs (FP) that have been selected, each corresponding to a different apogee radius for the injection orbit: 1.02 x 10^6 km for FP1; 1.06 x 10^6 km for FP2; and 1.10 x 10^6 km for FP3. The target inclination for all three programs is 5.59°. The FP that provides the longest continuous window of launch opportunities that satisfy all mission orbit requirements for a given day will be selected. The following analysis will only use FP2 to describe the results. The main effect of the various flight programs is to reduce the initial correction maneuver but does not affect the end science orbit.

The three target apogee altitudes were selected for the average distance from Earth to L2, approximately 1.5 x 10^6 km. However, this distance varies over the course of a year due to the eccentricity of Earth's orbit; in early January, when Earth is at perihelion, L2 is about 1% closer to Earth, and at apogee it is about 1% farther away.[3] This makes the correction maneuver more likely to overshoot the libration point in winter, and more likely to undershoot in summer.

Each of the three flight programs leads to a fixed insertion state defined in an Earth-centered, Earth-fixed (ECEF) coordinate system, and therefore the inertial position of this injection state varies with time as the Earth rotates during the daily launch window and as the orientation of the poles changes over the course of a year relative to the RLP frame. The annual effect can be seen by plotting the injection state in an Earth-centered RLP frame for a single time within the launch window over a full year, as shown in Figure 3(a), where every 30th day is highlighted in red.

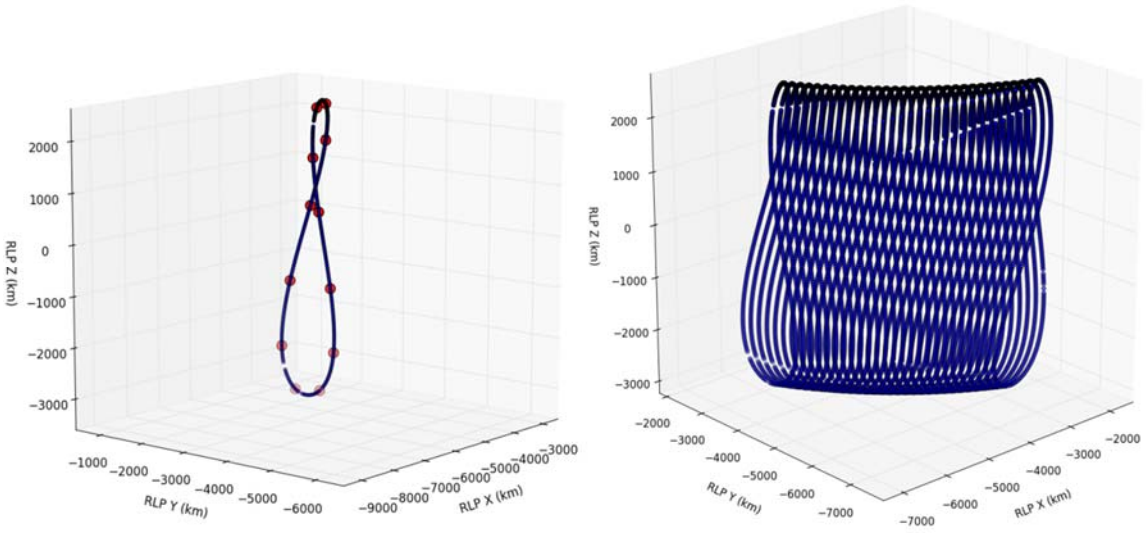

(a) **(b)**

Figure 3. Variation in ECEF injection position viewed in RLP (a) for 11:30 UTC launch over 1 year, and (b) for all launch epochs over 1 year.

This ‘figure 8’ shape results from the obliquity of the ecliptic and the eccentricity of Earth’s orbit around the Sun; these are the same underlying mechanisms which create the solar analemma, so it is not surprising that the resulting shapes are very similar.[4] Unlike the solar analemma, the ‘figure 8’ of injection positions is biased slightly below the ecliptic plane; the latitude of the Kourou launch site is 5.24° north of the equator, the inclination of FP2 is 5.59°, and the resulting injection latitude after 25 minutes of powered flight is 1.83° south of the equator.

Each epoch in the launch window has a similar, though not identical, shape. Figure 3(b) shows the variation for all epochs in the daily launch window over one full year. The opening of the launch window at 11:30 UTC is on the left side, and five minute intervals separate each curve until reaching 14:00 UTC on the right. Some geometrical properties of the resulting science orbit are readily explained from this pattern while other patterns are less intuitive, as will be seen in the following sections.

Transfer and Orbit Constraints

The injection state provided by Arianespace does not contain enough energy to deliver JWST to its operational LPO. This energy deficit is intentional to accommodate the possibility of over-performance by the launch vehicle. Due to JWST hardware constraints, it is impossible to remove energy from the transfer orbit, so if the launch vehicle were to deliver JWST at an energy level beyond its operational orbit, the observatory would fly beyond the libration point region and may not be recoverable. As such, a mid-course correction maneuver is required to add the necessary energy missing from the launch vehicle delivery to achieve an operational orbit. The mid-course correction is divided into three segments. Figure 4 shows the locations of the MCCs on a sample trajectory; MCC-1a is 12 hours after separation, MCC-1b is 2.5 days after launch, and finally MCC-2 is 30 days after launch. The cumulative ΔV budget for the three MCCs is set at 66.5 m/s.[2]

Several factors impose additional limitations that need to be considered during the mission design phase. The direction of thrust for the first two mid-course correction maneuvers is greatly restricted due to Sun exposure limitations. The sunshield is not yet deployed at this stage in the mission and therefore the instruments are only protected from the Sun in a narrow range of attitudes. As such, the angle between the direction of thrust and the JWST to Sun line must remain between 5 and 30 degrees. Fortunately, this direction restriction does not impose any severe constraints to the mission design process. The maneuver direction for the first two mid-course correction maneuvers is applied along the velocity vector, which is typically within the 5 to 30 degree restriction cone.[2]

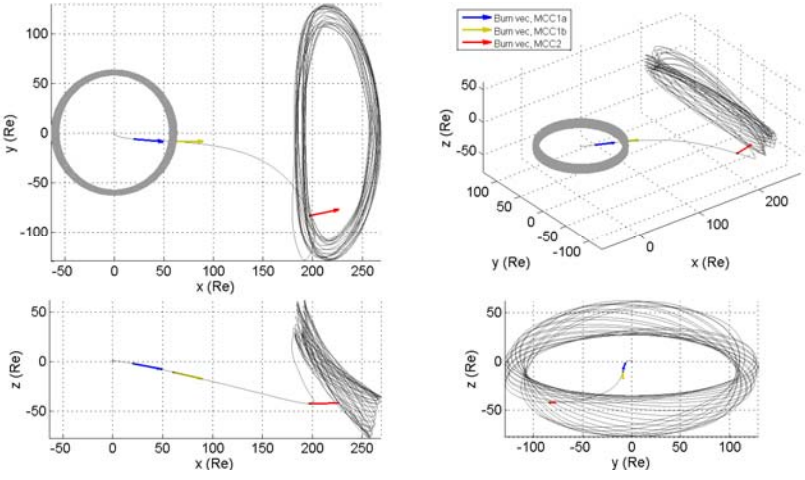

Figure 4. Sample trajectory showing location of mid-course correction maneuvers.

Also, JWST is never allowed to pass through the shadow of either the Earth or the Moon. Ensuring that the spacecraft is always in full Sun allows the thermal profile to remain consistent, and eliminates the need for any special power management if the solar array is not generating power.

Launch Window Overview

The launch window is defined by continuous time intervals between 11:30 and 14:00 UTC each day for which all the previous orbital constraints are met, and includes margin for model uncertainty (e.g. propulsion system performance). The previous launch window analysis demonstrated that over half of the launch readiness period (October thru December 2018) provides viable launch opportunities that satisfy all orbit requirements.[1] However, the geometry of the orbits varies significantly.

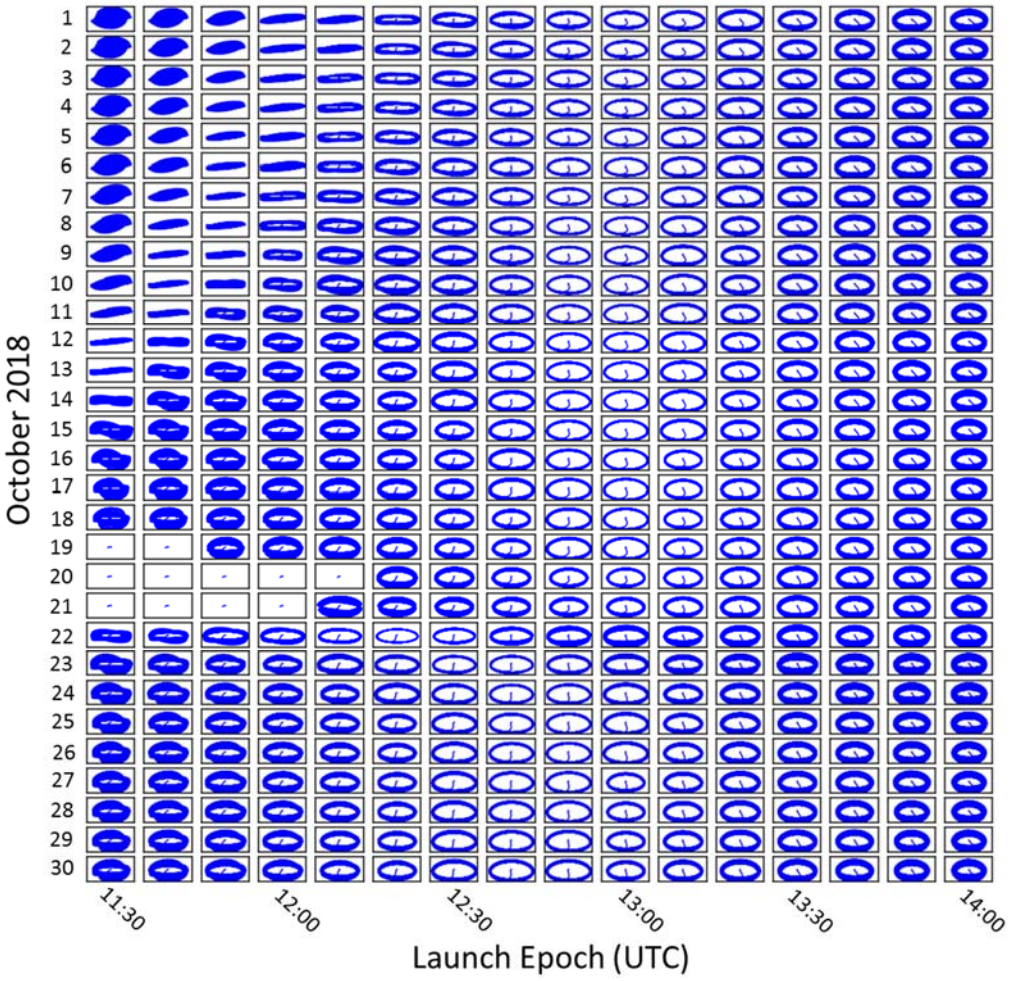

Figure 5. RLP YZ projection of JWST libration point orbits for October 2018.

Figure 5 shows the RLP YZ projection of all the orbits that are achieved during October 2018 with no constraint filtering applied; that is, all launch epochs that were able to enter orbit are displayed, even if they violate mission orbit requirements. Several patterns are evident. First, there are hourly variations during a given day launch window. Lissajous orbits are common early in the launch window, slowly transforming to halo orbits around 13:00, and finally becoming quasi-halos

at the end of the daily window. The monthly effects from the Moon are also apparent from the 19th-21st, where several opportunities at the beginning of the day are lost when gravitational perturbations are too large to be corrected with the available propellant. Halo orbits also appear earlier in the day than usual immediately after the lunar blackout period.

There are also variations on a yearly cadence, which are not apparent in the previous figure. In particular, the periods around the solstices, December 2018 and June 2019, do not present reasonable launch periods due to the larger number of orbit requirement violations. Inspection of a few such orbits typically indicates much larger orbit amplitudes around the December solstice, frequently exceeding the RLP Y and/or Z amplitude constraints. For the cases around the June solstice, the constraint violations mostly pertain to the required ΔV needed to achieve a science orbit. This is illustrated in Figure 6, which represents the transfer ΔV cost for all launch cases during the months of October and December 2018, and June 2019.

The combined ΔV for all three MCC maneuvers required to reach the LPO varies from 0 to 50 m/s. A period of several days exists each month when the required ΔV increases due to the third body influence of the Moon. December 2018 requires a lower ΔV to achieve its LPO, but the average orbit size violates JWST requirements too frequently; conversely June 2019 requires the most ΔV to achieve the LPO. October 2018 was selected as the start of the launch readiness period as it requires only a moderate ΔV while resulting in reasonable orbit geometries for many launch times. The following sections will explore the dynamics that drive these results.

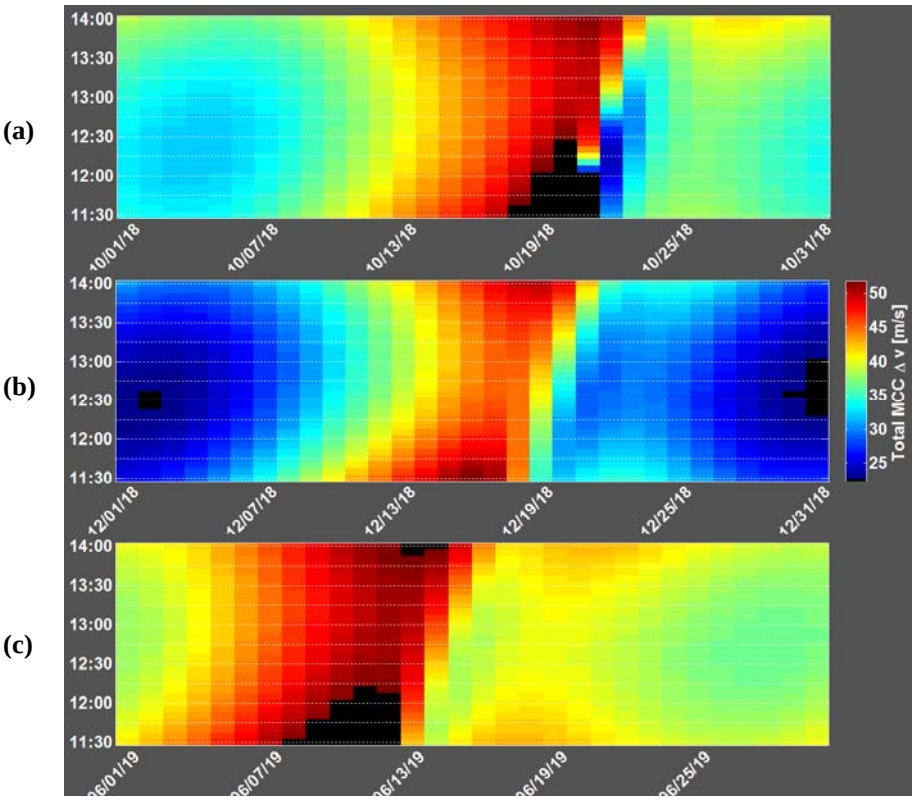

Figure 6. Total ΔV required for launch in (a) October 2018, (b) December 2018, and (c) June 2019. All cases use FP2 from Arianespace.

RELATIONSHIP BETWEEN LAUNCH EPOCH AND SCIENCE ORBIT GEOMETRY

As discussed in the previous section, the science orbit geometry (and other orbital characteristics) varies in a complex fashion on hourly, daily, monthly and yearly rhythms. The geometry of the science orbit depends on several factors, including the launch epoch, the location (phase) of the Moon and its gravitational influence on the transfer trajectory, as well as longer period effects due to the eccentricity of Earth's orbit around the Sun. This section explores the relations between these factors by leveraging the geometry of the problem and the well-known results from the CR3BP. In particular, we show that these variations can be understood as deterministic motion of the insertion state on the stable manifold of the libration point region. To proceed, the next paragraphs further explores the effect of the Earth's motion in the RLP frame while the remainder of the section focuses on the approximation of the transfers and science orbits using the CR3BP.

From ECEF to RLP

As was discussed in the previous section, the launch trajectory is fixed in the ECEF frame, but creates shifted 'figure 8' in the Earth-Sun synodic frame. The daily launch window time span leads to an almost linear drift in right ascension (RA) and declination (DEC) in the synodic frame due to the angle between the Earth's equator and the ecliptic plane.[*] RA is the angle measured in the RLP XY plane relative to the X axis, and increases with positive rotation about the Z axis; DEC is the angle above or below the XY plane. Note in particular that the start of the launch window is close to noon UTC and thus corresponds to a near maximum declination for each day from June to December and a minimum for the other half of the year. As a consequence, while the obliquity of the ecliptic is fixed, the relative declination of the launch insertion varies between $\pm(\varepsilon+\lambda)$, where λ is the latitude of the insertion point in the ECEF frame (-1.83°), and ε is the obliquity of the ecliptic (23.4°). The declination varies slowly each day, creating the amplitude of the 'figure 8' over a year. The width and actual 'figure 8' shape is due to the eccentricity of the Earth's orbit around the Sun. Indeed, compared to the mean Sun, the synodic X axis will lead the direction of the mean Sun for half of the year (centered on the Winter solstice) and lag the mean Sun during the other half (since the angular frequency is smaller than the mean motion when the Earth is near aphelion). This qualitative picture can be more accurately captured in the sequence of rotations going from the ECEF to the synodic frame:

$$\vec{r}_{Synodic} = R_1(\varepsilon).R_3(\theta_{hour}).\vec{r}_{ECEF},$$

where $\theta_{hour} = (2\pi - n_E).t_{GMT}$ is the hour angle, n_E is the mean motion of the Earth around the Sun. The symbols R_1 and R_3 represent the elementary rotations about the first and third axis, respectively.

In addition to the above variations, the motion of the Earth-Moon barycenter also creates monthly fluctuations in the insertion states and resulting orbits. Indeed, the RLP frame used in the science orbit definition (and in which the libration point dynamics is measured) is defined relative to the Sun and Earth-Moon barycenter line. This is illustrated in Figure 7. This can be approximated by expressing the motion of the Earth around this barycenter as a nearly circular orbit with a major axis of about 9200 km and period equal to the Moon's period (relative to the synodic frame) around the Earth.

In particular the Earth motion can be approximated in terms of the Moon's orbital elements relative to the Earth as

[*] Which is spanned by the X, Y-axis of the synodic frame and the fact that UTC is kept very closely to a mean Sun time; that is, a mean synodic frame.

$$\vec{r}_{Earth}(t) \cong R_3(-\Omega_{Moon}).R_1(-\iota_{Moon}).R_3(\pi - \omega_{Moon}).\vec{r}_{2BP}(t),$$

where

$$\vec{r}_{2BP}(t) = [-R_{Earth}.\cos(M_{Moon}), -R_{Earth}.sin(M_{Moon}), 0]^T.$$

M_{Moon} is the mean motion with a period of a lunar month, and R_{Earth} is the radius of the Earth's orbit around the Earth-Moon barycenter. As a result, the ECEF insertion position is expressed in the RLP frame as:

$$\vec{r}_{RLP} = R_{RLP}.\{R_1(\varepsilon).R_3(\theta_{hour}).\vec{r}_{ECEF} + \vec{r}_{Earth}(t)\},$$

where $R_{RLP} = R_3(\upsilon - \upsilon_0)$ represents the rotation between the ecliptic and the RLP frame and is a function of the Earth-Moon barycenter true anomaly around the Sun, υ.

These transformations, thus clearly show the three main frequencies entering in the motion of the fixed ECEF insertion state when viewed from the RLP frame: hourly (θ_{hour}), monthly (M_{Moon}) and yearly (υ). The daily variations are due to the combination of the monthly and yearly variations.

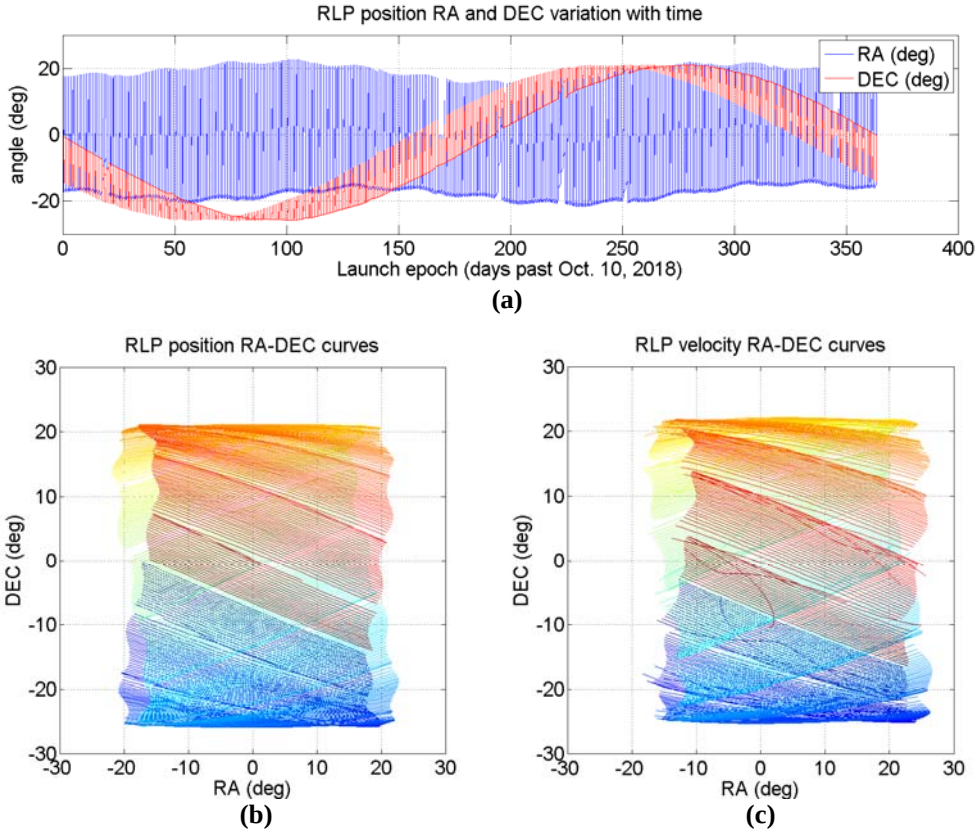

Figure 7. Insertion positions in the RLP frame. (a) Time history of the RLP RA and DEC, showing the yearly periodicity of DEC and monthly variation in RA. (b) RA, DEC view showing the variation in the baseline 'figure 8' for position. Points with the same color correspond to launch epoch occurring on the same day. (c) RA, DEC view showing the variation in the baseline 'figure 8' for velocity.

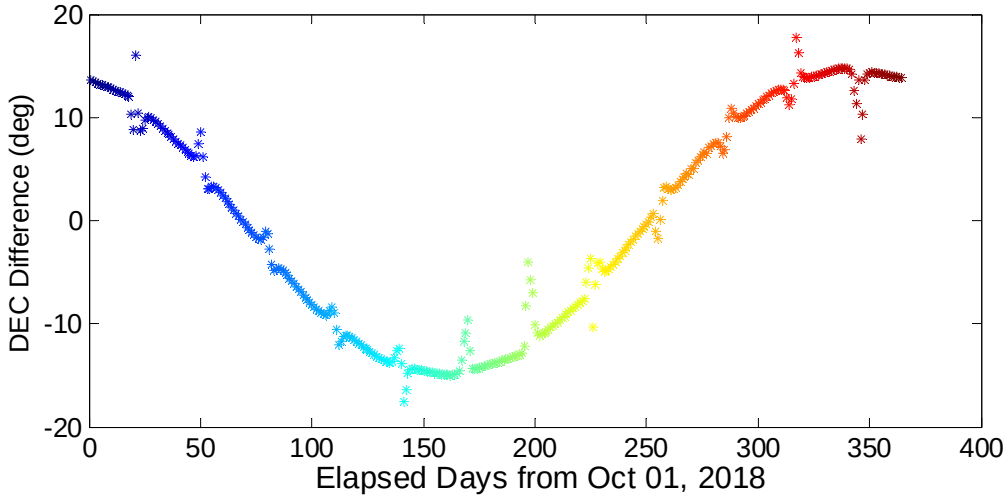

Figure 8. Difference in DEC of velocity after MCC-1a between start and end of daily launch window.

We can also deduce from this analysis that node regression of the Moon's orbit will lead to a small difference in the monthly variations which can be observed in the extrema of the declination of the insertion state in the RLP over the 10 year span of the mission. Since we are concerned here with the main mechanism, this has not been investigated further. However, we should note that the velocity perturbations due to the Moon are more strongly marked when the Moon at launch is in the waxing gibbous to full phase. This is illustrated by plotting the RA and DEC of the post-MCC-1a spacecraft velocity vector in RLP coordinates, shown in Figure 7(c). A few days per lunar month have diverging curves in this (RA, DEC) space, indicating the unusual MCC-1a correction maneuver needed to place the spacecraft on a libration point orbit transfer when the Moon is in the way.

To identify the days when the Moon has the largest influence, the difference in declination between the first and last launch opportunities was computed for each day. As previously mentioned the declination will vary sinusoidally between $\pm(\varepsilon+\lambda)$, so any point that deviates from this trend indicates that the lunar perturbation is present. Figure 8 shows six or seven days of every month are affected by the Moon. The average RA in RLP of the Moon at launch on the first day with significant lunar perturbations is -65°, and the average RA on the last perturbed day is 19°.

Near Ballistic Transfers

In order to further investigate the relation of the JWST transfers to stable manifolds of LPOs, we note first that the transfers are close to being ballistic post-MCC-1a. The launch vehicle provides the majority of the energy necessary to deliver the observatory to an operational orbit; however, it is not quite enough to inject onto a stable manifold and achieve a science orbit at L2. As stated earlier, the lack of necessary energy is intentional to prevent the launch vehicle from overshooting the L2 region and losing the spacecraft into a heliocentric orbit. As seen in Figure 9, even with the decrease in necessary energy the observatory is almost on a ballistic trajectory toward an operational orbit at L2. The post-MCC-1a state, when performed at 100%, demonstrates the ballistic nature of the overall mission design.

In practice, MCC-1a will not provide 100% of the required energy for the same reason that the launch vehicle does not target a direct transfer to the libration point. The effects of a 5% bias down are evident in the green trajectory in Figure 9, which falls back to Earth just before the first station keeping maneuver would be performed. By performing the additional two MCC maneuvers, the

required energy is achieved, as seen through the blue trajectory. An interesting observation is that the trajectory based off a single MCC maneuver at 100% and the trajectory resulting from three MCC maneuvers (two biased down) are nearly identical. The only cost is the small ΔV penalty associated with delaying MCC-1b until 2.5 days.

The Jacobi constant for each of these trajectories in the realistic model was also evaluated. Figure 10 shows the variation in this integral of motion over two different regions: the transfer from Earth to L2, and one full year in the LPO. As can be observed, the Jacobi 'constant' is quite variable in this case.

The sharp variation at the beginning of the transfer in Figure 10(a) results from the difference in modeling the CR3BP dynamics near the Earth-Moon barycenter; in the full model the acceleration is split between the Earth and Moon's gravitational fields. However, once in the libration point region and far from the Earth and Moon, the value settles to a gentle variation with small amplitude. This oscillation has a one-year period and can be accounted for by the eccentricity of the Earth-Moon barycenter's orbit around the Sun.

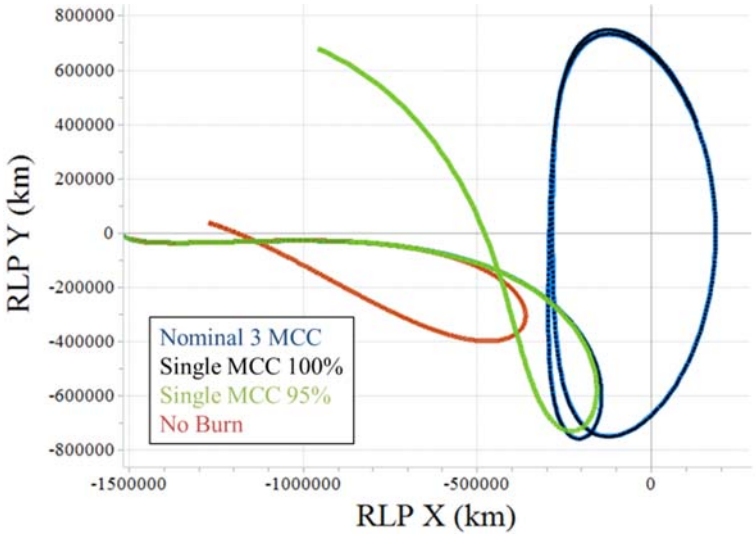

Figure 9. Transfer trajectories with various MCC maneuver magnitudes.

To account for the varying Jacobi value, both from MCC-1a to the libration point while in the LPO, the average was computed over one full year in orbit starting 6 months after launch. These values were then used to generate orbits at the same energy level in the CR3BP. Unfortunately, there was a significant difference in the amplitudes of these orbits compared to the orbits in the full ephemeris model. While the Jacobi constant would seem to provide the easiest method of transitioning between the simplified and full dynamical models, later sections will show that a match in velocity direction is sufficient to generate matching orbits, after a velocity correction is applied. With these results, the next step consists of matching these transfers with CR3BP orbits whose type and structure are more firmly characterized.

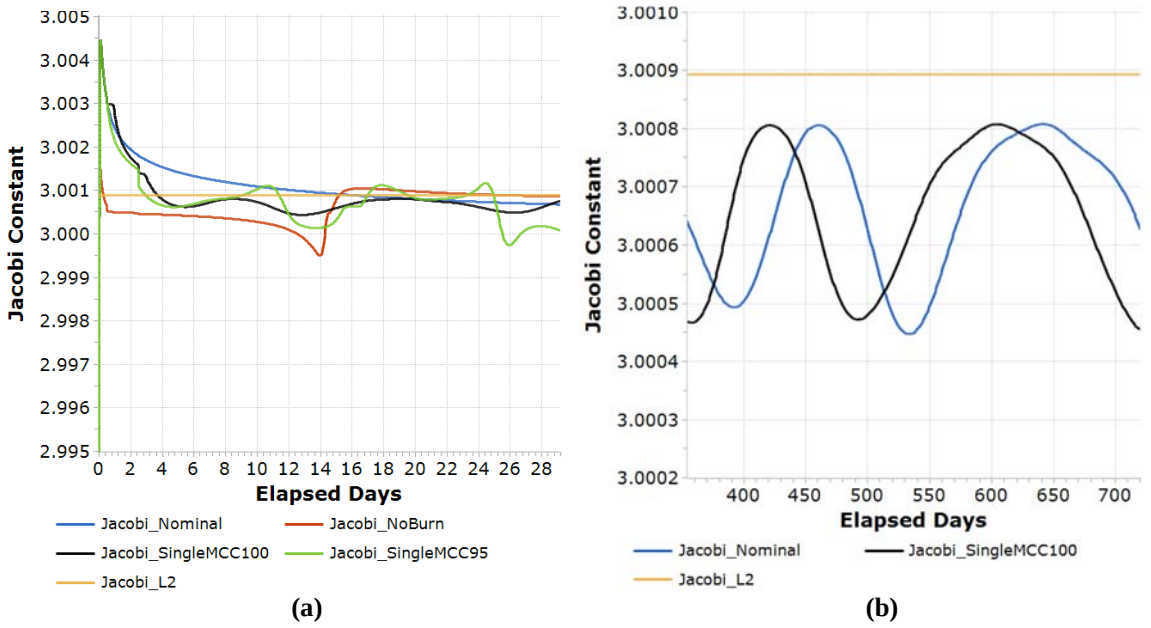

Figure 10. Jacobi constant for various MCC magnitudes. (a) Transients observed in vicinity of Earth and Moon. (b) Variations are much smaller once around the libration point.

Review of the CR3BP libration point dynamics

The libration point region of interest consists of a set of periodic and quasi-periodic orbits that oscillate around the L2 point without encircling the Earth, Sun or Moon. The most relevant families of periodic orbits for this discussion are the planar and vertical Lyapunov families and halo orbits. Figure 11 presents an overview these families of periodic orbits. Note that for a given Jacobi constant value, *C*, both northern and southern halo orbits exist and correspond to different direction of motion when observed from the Earth (clockwise vs. counter-clockwise, respectively). As was observed in the previous section, both of these cases are possible JWST orbits.

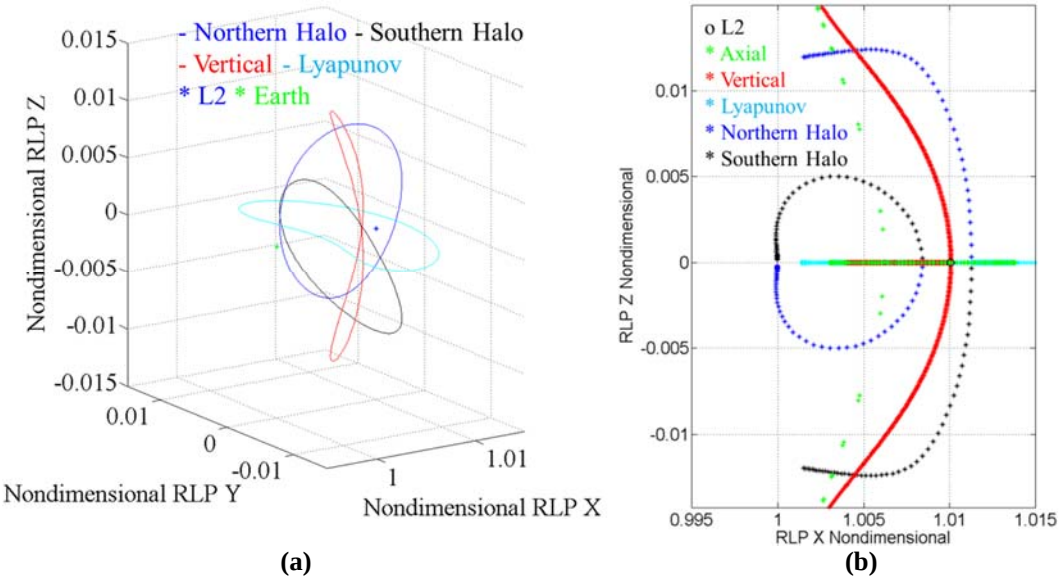

Figure 11. Periodic orbit families in the CR3BP L2 region. (a) Selection of sample periodic orbits. (b) Synthetic representation in terms of apsis conditions.

While periodic orbits represent only a very small set of LPOs, they form the basis for the quasi-periodic orbits. Quasi-periodic orbits notably exist around these families, and are typically classified as quasi-halo orbits or Lissajous orbits. These latter orbits can be of small amplitude and stay near the corresponding planar Lyapunov orbit at the same energy (quasi-Lyapunov orbits) or of large amplitude, quasi-vertical orbits. These orbits comprise the set of CR3BP orbits that represent JWST science orbits. Note in particular, that at the range of Jacobi constant of the JWST transfers, the periodic orbits in these libration point regions are quite large. Figure 12(a) shows the relative size of the halo orbits, the zero velocity curves and the Moon's orbit, while Figure 12(b) indicates the size of the set of orbits that escape the Earth-Moon Hill's region (red and blue points).

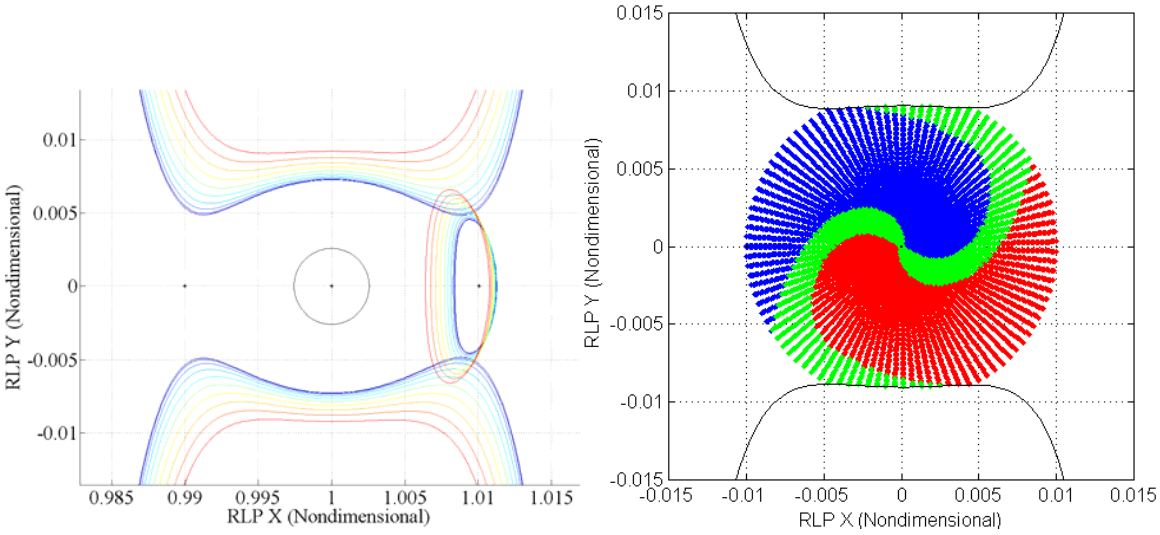

(a) **(b)**

Figure 12. Relative size of orbits and escape set at the Jacobi constant of interest. (a) zero velocity curves and corresponding halo projections;(b) periapsis point colored by transit behavior: red for escaping orbits through L2, blue for escape through L1 and green for orbits that fall back toward the Earth-Moon system for at least one revolution.

At the energies considered, most of these orbits are unstable and present a set of (ballistic) asymptotic orbits that either converge to the given orbit in forward or backward time (stable and unstable manifolds, respectively). Figure 13 presents sample trajectories in the stable manifold of a halo orbit. Other LPOs have corresponding stable manifolds, including quasi-periodic orbits. The stable manifold trajectories provide direct transfer from the Earth vicinity to the libration point region, and are thus the CR3BP orbits corresponding to the JWST transfers. The manifold structure can thus be used to better understand the variation in the observed JWST science orbits.

As can be observed from Figure 13, the stable manifold to a halo orbit forms a tube structure in three dimensions. Trajectories along the manifold are computed by first selecting a sequence of states on the periodic orbit over a base period, then performing an eigenvalue analysis of the corresponding monodromy matrix to generate initial states perturbed along the computed eigenvectors.[5,6] Thus, the manifold can be parameterized by an angle that represents the selection of initial state in this algorithm (namely, $\theta = 2\pi(t/T)$, where t represents the time used in the computation and T the period of the orbit) and the time along the manifold orbit from the computed initial point. The intersection of the manifold with a Poincaré section reveals a closed loop of possible trajectories, as we will be doing in the following.

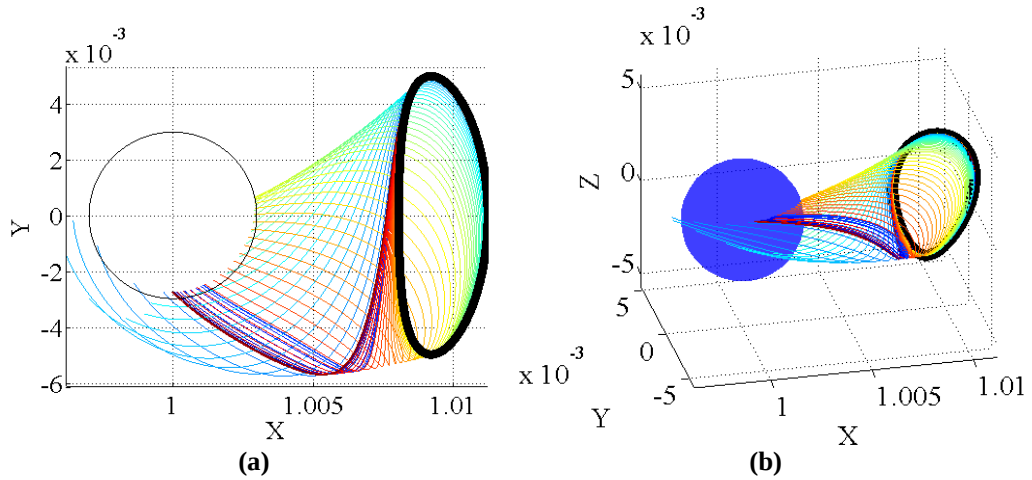

Figure 13. Stable manifold of a sample periodic orbit.

In general quasi-periodic orbits require two angles (plus the time along each orbit) to be parameterized and will thus appear as tori shapes on Poincaré sections. More interestingly, the manifolds of the various LPOs are organized as a boundary of transit orbits and can be shown to be equivalent to a 4-dimensional sphere for a fixed Jacobi constant value.[7] In particular, given a point on a manifold, the set of velocities leading to other manifold orbits (with the same energy) is a circle. Alternatively, for a given velocity direction, the set of position leading to manifold transfers is a closed curve, and present thus a maximum out-of-plane component. For example, in the case of a halo orbit, the intersection of the manifold with the RLP (X,Y)-plane does not occur at a zero inclination (relative to the RLP frame) and an injection state having a small inclination cannot thus reach a halo orbit from that location. This is in contrast to the planar Lyapunov orbits, which do not present any out-of-plane component in any intersection. These effects will be captured in greater detail in the next section.

Matching JWST Transfer Orbits

In order to relate the above manifold orbit organization to the JWST orbit variation, we must thus match the transfers to corresponding manifold orbits. As was seen in the previous section, the JWST transfers are fairly close to ballistic and such a match should thus be possible. The following paragraphs discuss the approach used to perform such an operation.

Choice of matching conditions. The first step in matching orbits between two different models is to agree on the interface. Given the near ballistic nature of the transfer post-MCC-1a or post-MCC-1b, these post-maneuver states are thus considered (rather than the insertion states analyzed previously) as matching conditions. As was noted previously, the MCC-1a and MCC-1b maneuvers are only applied in the direction of the observatory velocity and thus only change the value of the Jacobi constant in CR3BP approximation. In particular, the post-MCC-1a position is very close to the ballistic position obtained from the insertion states and the RA, DEC variations of both post-MCC-1 states follow a similar 'figure 8' variation as was discussed in the previous section.

In order to match invariant manifold of LPOs to these post-MCC-1a states, one can look at comparing the manifold intersection with the selected post-MCC-1a sphere (chosen as having 70 Earth radii). In particular, since the position magnitude is fixed, matching in position can be measured as distance in RA and DEC differences on that sphere. Figure 14, for example, shows the intersection of a manifold associated with a halo orbit with all of the possible (RLP transformed)

JWST transfer state when they intersect a sphere of 70 Earth radii (referred to as injection states). The black stars seen on this plot represent the RLP transformed injection states ('figures 8'), while the color stars represent intersections of the manifold. From this representation it is clear there is a large position and velocity continuity overlap between the manifold and the post-MCC-1a states; however, it is not clear if the position and velocity continuity occurs for the same transfer conditions. In other words, a single injection state needs to match the same position and velocity manifold intersection in order to take advantage of the direct transfer.

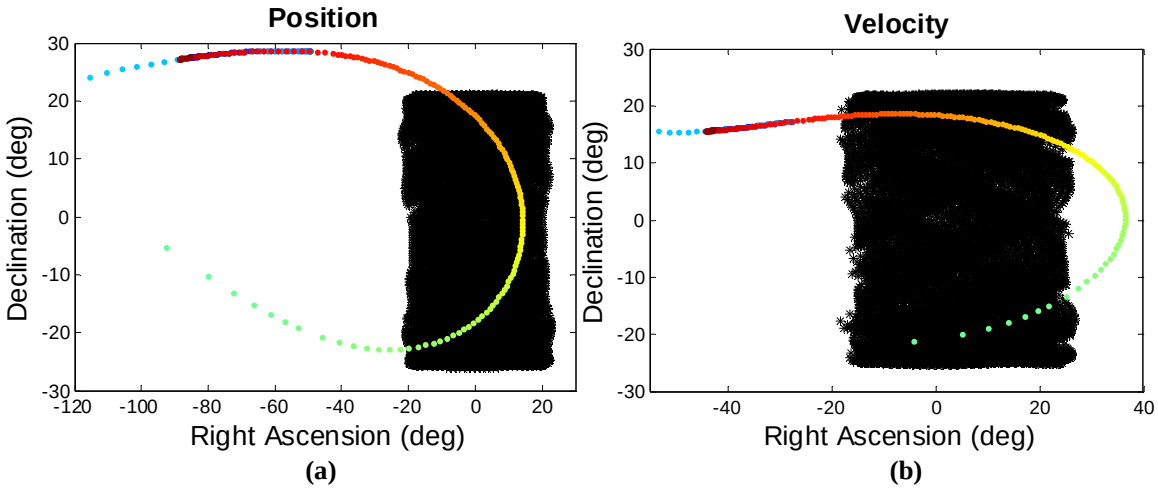

Figure 14. Intersecting injection states with the manifold of a halo orbit at 70 Re in (a) Position, and (b) Velocity.

With these interface choices, we are thus led to a set of matching condition between the injection states and the manifold intersection states:

$$\begin{cases} RA\left(\vec{r}_{injection}\right) = RA\left(\vec{r}_{manifold}\right); \; DEC\left(\vec{r}_{injection}\right) = DEC\left(\vec{r}_{manifold}\right) \\ RA\left(\vec{v}_{injection}\right) = RA\left(\vec{v}_{manifold}\right); \; DEC\left(\vec{v}_{injection}\right) = DEC\left(\vec{v}_{manifold}\right) \end{cases}$$

These equations represent a system of four equations in four unknowns (three manifold parameter and the Jacobi constant) and a finite set of solutions can be expected for each injection condition. While it theoretically possible to obtain several manifold orbits with the given position and velocity direction (thus differing in magnitude only), the local search in C near the average Jacobi constant observed for the particular injection condition leads to a single solution.

Note that in as much as the set of injection states is parameterized by the launch epoch, the CR3BP solutions can be tied to a particular launch epoch. Alternatively, one could use the simplified model used to describe the 'figure 8' states and use the hour angle, Moon's mean anomaly and Earth mean anomaly to approximate this set of injection states to recover the relative geometry of the Sun-Earth-Moon system that leads to a particular science orbits.

Matching periodic orbits. For periodic orbits, the stable manifold intersections are parameterized by only two parameters, θ and C. Thus, no exact solution to the above equations is to be expected in general. However, one can look at the closest manifold transfer from a given state to provide some insight into the observed orbit type variations. Therefore, the above equations are cast as a minimum distance problem, where the distance if defined in the 4-dimension Euclidean distance between the vectors:

$$X_{inj} = \left(RA_{\vec{r}_{inj}}, DEC_{\vec{r}_{inj}}, RA_{\vec{v}_{inj}}, DEC_{\vec{v}_{inj}}\right) \quad and \quad X_{man} = \left(RA_{\vec{r}_{man}}, DEC_{\vec{r}_{man}}, RA_{\vec{v}_{man}}, DEC_{\vec{v}_{man}}\right).$$

The numerical approximation to the cost function is shown in Figure 15(b) where the colors match the manifold orbits shown in Figure 15(a). As can be observed, a few points exist where the position and velocity continuity between the post MCC-1a injection state and the manifold is very nearly satisfied. Ideally the post MCC-1a state at the computed epoch, should fall into a near halo orbit with the characteristics of the reference orbit from the CR3BP when propagated forward in time.

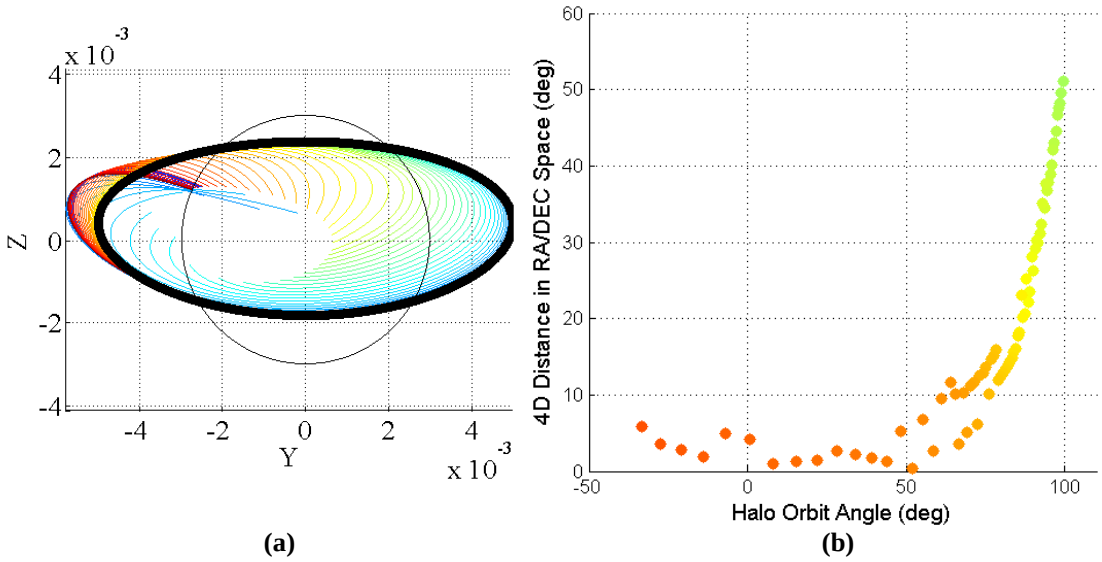

(a) **(b)**

Figure 15. Matching position and velocity with a stable manifold of a halo orbit. (a) RLP (Y,Z)-projection of halo orbit and manifold used showing coloring scheme used. (b) Distance in 4D (RA, DEC) space showing minimum distance around θ = 50°.

To test this theory, the injection state with the best position and velocity matching is propagated forward in time, along with a station keeping algorithm, in a full ephemeris model to determine the characteristics of the resulting operational orbit. Figure 16(a) visualizes the resulting orbits. The red orbit was generated in the CR3BP model while the blue orbit is the ephemeris created in a full force model (The lunar orbit is shown in black for scale). Visually, the two orbits are nearly identical. To further confirm the matching, Figure 16(b) shows the X, Y, and Z amplitudes throughout the span of the ephemeris. The dotted lines correspond to the maximum Y and Z amplitudes from the CR3BP model. As can be observed, the two orbits are nearly identical. The Y and Z amplitudes match closely.

The above process can be repeated for a range of Jacobi constants and families of periodic orbits. In particular, Figure 17(a) shows the minimum 4D distance from any post-MCC-1a position for northern halo (blue), southern halo (red), and Lyapunov (green) orbit families, where increasing family member number correlates to increasing amplitude of the associated LPO. In Figure 17(b), these positions of these family members with a 4D separation less than 1 degree are overlaid on the positions of all post-MCC-1a states. Note that only northern and southern halo orbits meet this criterion; Lyapunov orbits match the insertion positions closely but have a large difference in velocity, and the opposite is true for vertical orbits. The halo orbit family members with the smallest separation from insertion states have a Jacobi constant between 3.00075 and 3.00080. The closest matches for the halo orbits with real insertion states tend to occur in the middle of the daily launch

window, with southern bias occurring at negative declination, and northern bias at positive declinations. Referring back to Figure 7(a) the seasonal relationship becomes apparent, as these declinations are predominant in the winter and summer, respectively.

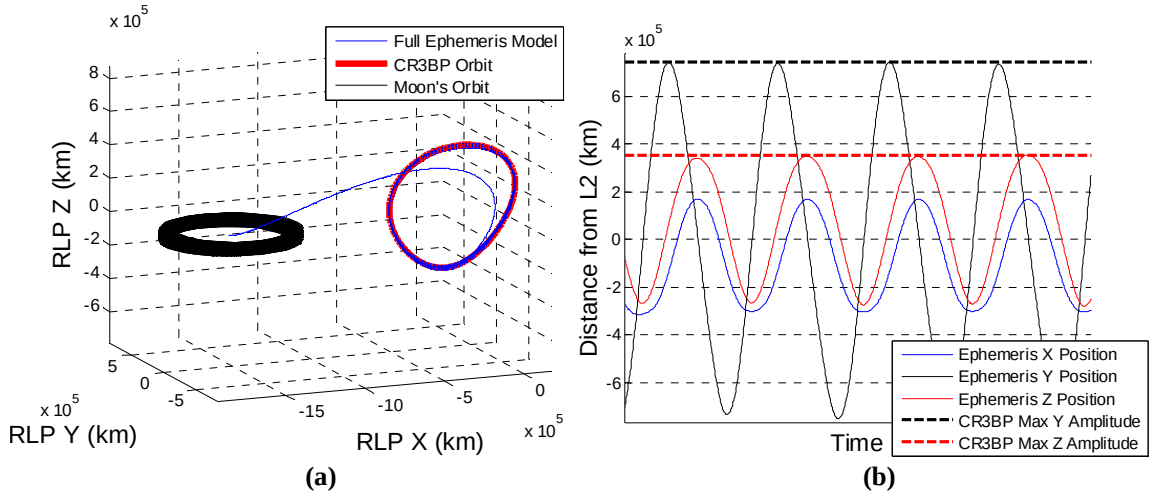

Figure 16. Overlay of matched CR3BP with the full force model JWST transfer. (a) 3D view in the RLP frame; (b) comparison of the component amplitudes.

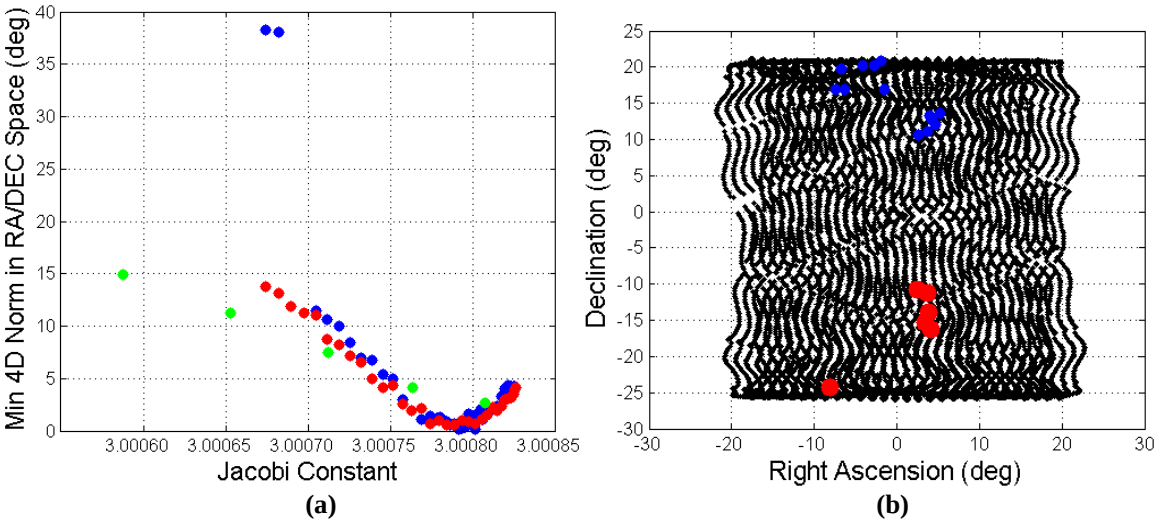

Figure 17. Injection state differences between CR3BP and ephemeris model. (a) Minimum 4D difference in (RA, DEC) space for members of halo, vertical, and Lyapunov families. (b) Northern and southern halo orbit states with 4D distance less than 1 degree compared to post-MCC-1a positions.

This shows that there is a strong relationship between the declination post-MCC-1a and the bias of the science orbit. This is further confirmed by examining not just the nearest matches in 4D (RA, DEC) space, but looking at the patterns established when observing the declination space in both position and velocity, as shown in Figure 18. The blue and red sections in the figure correspond to the northern and southern halos, respectively. The purple region maps the vertical family. The origin corresponds to the planar Lyapunov family. Only a very narrow set of conditions exists in declination space that would result in a periodic halo orbit. This small declination intersection subset explains the existence of numerous quasi-halo and Lissajous orbits, as observed earlier in Figure 5.

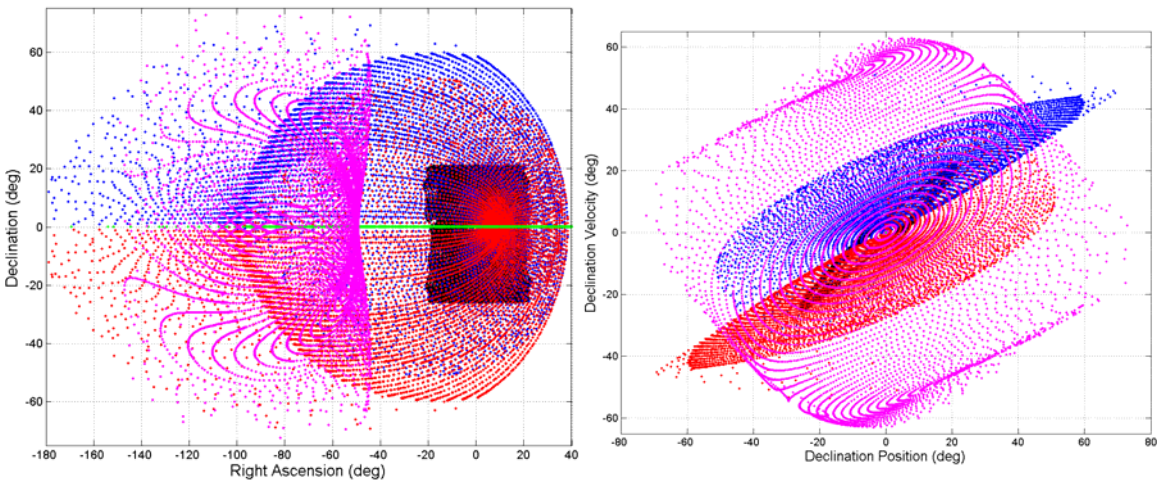

(a) **(b)**

Figure 18. Injection state differences between CR3BP and ephemeris model at post-MCC-1a epoch. (a) (RA, DEC) space position. (b) (Pos. DEC, Vel. DEC) space.

Throughout this investigation, much effort has been placed into matching halo and quasi-halo orbits. Very little attention has been given to Lissajous orbits as using the manifold intersection technique for non-periodic orbits is difficult. Because Lissajous orbits are an extension of the planar Lyapunov family, reasoning suggestions that the Lissajous family would exist in (RA, DEC) space near the existence of the Lyapunov family. In position and velocity declination space shown in Figure 18(b), the Lyapunov family is located at the origin. To test the idea that the Lissajous family would exist near the Lyapunov family, the post MCC-1a state closest to the origin was selected and propagated in a full ephemeris model. The resulting orbit, shown in Figure 19, appears to be a Lissajous orbit.

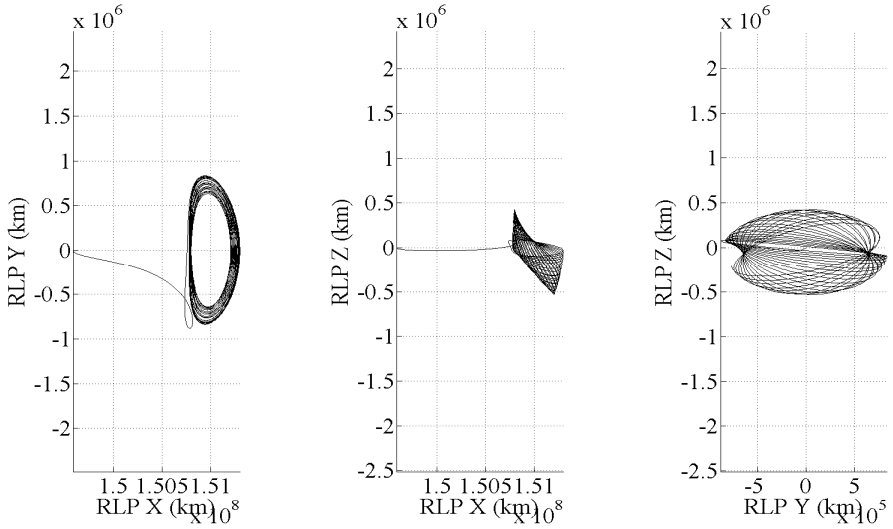

(a) **(b)** **(c)**

Figure 19. Lissajous trajectory resulting from closest intersection with Lyapunov state in (Pos. DEC, Vel. DEC) space.

Matching general transfers. In the general case, the matching condition can be solved by dichotomy on the velocity magnitude, in a similar process as the computation of MCC-1a and the

algorithms explored by Villac and Scheeres.[7] In particular, given RA and DEC for position and velocity, the change in velocity magnitude will lead to a change in transit orbit type: from non-transit at small velocity magnitude values to transit orbits at higher speed. Refining the velocity magnitude at which the orbit type change occurs leads to a trajectory on the stable manifold to a libration point orbit. This process has been carried out for the set of injection conditions and Figure 20(a) shows the discrepancy in Jacobi constant between the average observed on ephemerides for JWST orbits and the differentially corrected orbit in the CR3BP.

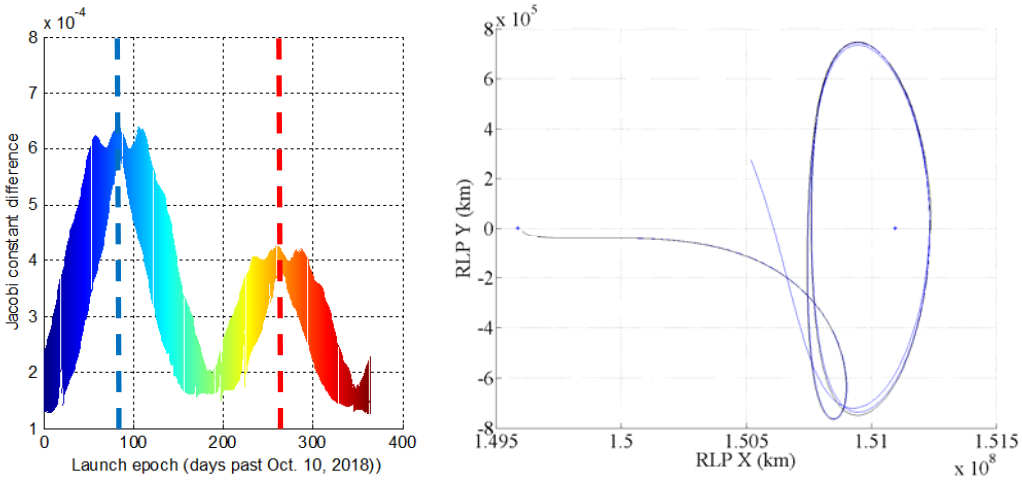

Figure 20. Differential correction results. (a) Jacobi constant differences between JWST average value and CR3BP corrected state. The dashed blue and red lines indicate the Winter and Summer solstices respectively. (b) Plot of matching orbits for the largest difference case.

As was noted before, there is a discrepancy in the appropriate definition of the Jacobi constant in the ephemeris model. However, the largest differences indicate some general trend: the trajectories appear to be further away from a ballistic transfer around the winter and summer solstices (days 75 and 255 in Figure 20(a), corresponding to Dec. 16, 2018, and Jun. 14, 2019, respectively) where large sizes of orbits are also observed. Conversely, the spring and autumn present smaller corrections that also led to close match to periodic orbits as was observed in the previous paragraph.

Note that even in the case of the largest discrepancies in Jacobi constant, the orbits do match the JWST orbits very closely, as shown in Figure 20(b). Thus, even though the Jacobi constant only partially represent the JWST orbits, the differential correction process converges for each orbit, validating and enlarging the explanation put forth earlier: the variation in the observed JWST science orbit is due to the varying insertion condition in the RLP frame. The motion of this insertion condition is due to having a fixed insertion condition in the ECEF frame and launch opportunities is more likely to satisfy the mission constrain when the insertion state is closer to the manifold of a libration point orbit.

CONCLUSION

The analysis in this paper has shown the CR3BP model is a useful tool to extract many of the relationships between the launch epoch and the science orbit geometry for JWST. The fixed insertion position in ECEF leads to hourly variations as the Earth rotates, monthly variations as the Earth and Moon orbit their barycenter, and yearly variations as the Earth orbits the Sun. Creation of periodic orbits in the simplified model provides insight into the types of orbits that are achieved.

The predominance of quasi-periodic trajectories occurs as most JWST insertion states do not intersect exactly with invariant manifolds of periodic orbits created in the CR3BP.

In terms of mission design, future spacecraft operated at L2, or even L1, can apply the lessons learned from this analysis of possible JWST orbits. Many libration point orbiters target a fixed reference orbit by having the launch vehicle target a fixed state in the RLP frame. This shifts the complexity of the trajectory design from the spacecraft to the launch vehicle, however for missions with relatively few constraints on the type of libration point orbit, a launch vehicle state fixed in ECEF may be a simpler solution. For spacecraft with a larger ΔV budget and/or fewer attitude constraints, it may be possible to target orbits with a smaller range of variations by designing the correction maneuvers appropriately.

ACKNOWLEDGMENTS

a.i. solutions' contribution to this work was performed under NASA contract #NNG14VC09C.

REFERENCES

[1] W. Yu and K. Richon, "Launch Window Trade Analysis for the James Webb Space Telescope," *24th International Symposium on Space Flight Dynamics*, 5-9 May 2014.

[2] J. Petersen, J. Tichy, G. Wawrzyniak, and K. Richon, "James Webb Space Telescope Initial Mid-Course Correction Monte Carlo Implementation using Task Parallelism," *24th International Symposium on Space Flight Dynamics*, 5-9 May 2014.

[3] L. Hiday, "Optimal Transfers between Libration-Point Orbits in the Elliptical Restricted Three Body Problem," Ph.D. Dissertation, Aeronautics and Astronautics Dept., Purdue Univ., West Lafayette, Indiana, 1992.

[4] P. Lucht, "Sun-Earth Kinematics, the Equation of Time, Insolation and the Solar Analemma," 2013.

[5] W. Koon, M. Lo, J. Marsden, and S. Ross, "Dynamical Systems, the Three-Body Problem, and Space Mission Design," 2011.

[6] V. Szebehely, "Theory of Orbits: The Restricted Problem of Three Bodies," *Academic Press*, New York, 1967.

[7] B. Villac and D. Scheeres, "A Simple Algorithm to Compute Hyperbolic Invariant Manifolds Near L1 and L2," *AAS/AIAA Space Flight Mechanics Meeting*, February 2004.